JOURNAL OF SOLID STATE CHEMISTRY **141,** 99–104 (1998)
ARTICLE NO. SC987923

Preparation, Crystal Structure, and Reducibility of K_2NiF_4 Type Oxides $Eu_{2-x}Sr_xNiO_{4+\delta}$

Lou Hui,*,[1] Chen Ping,† Ge Yuping,† Lu Yueqing,‡ Lü Guanglie,§ Xü Yuanzhe,* and Ma Futai†

*Department of Chemistry, Zhejiang University, Hangzhou 310027, China; †Department of Chemistry, Hangzhou University, Hangzhou 310028, China; ‡Department of Biochemistry, Shaoxing Normal College, Shaoxing 312000, China; and §Central Laboratory, Hangzhou University, Hangzhou 310028, China

Received October 27, 1997; in revised form June 1, 1998; accepted June 2, 1998

K_2NiF_4 type compounds $Eu_{2-x}Sr_xNiO_{4+\delta}(0.5 \le x \le 1.2)$ have been prepared by a citric acid complex decomposition method. Rietveld refinement of the powder X-ray diffraction data showed that there was a crystal system transformation from orthorhombic *Fmmm* to tetragonal *I4/mmm* at around $x = 0.6–0.7$. The Sr substitution caused a drastic shift of the O_{II} ions along the *c*-axis from Eu(Sr) toward Ni while scarcely affecting the NiO_4 network in the basal plane. The Jahn–Teller distortion of the NiO_6 octahedron decreased while the percentage of Ni^{3+} increased with increasing *x*. The variation of the higher peak temperature on the TPR profiles with *x* are opposite to the variation of the cell parameters *c*. © 1998 Academic Press

INTRODUCTION

K_2NiF_4 type rare earth complex oxides A_2BO_4, consisting of alternating layers of ABO_3 perovskite and AO rock salt structures along the *c*-axis (Fig. 1) (1–4), have been widely studied for their high-temperature stability, two-dimensional conductivity, and catalytic properties (1–6). These properties are closely related to the types of ions *A* and *B*, the valence state of the transition metal ions *B*, and the crystal structure of the compounds (7, 8).

According to the tolerance factor limitation ($t = r_A/r_B$) proposed by Ganguli (9), neodymium is the smallest rare earth metal ion which can form a K_2NiF_4 type lanthanide nickelate (10, 11). Since europium is smaller than Nd, it cannot form a K_2NiF_4 type nickelate compound. By partial substitution of Eu^{3+} with larger ions such as Sr^{2+}, however, K_2NiF_4 type compounds $Eu_{2-x}Sr_xNiO_{4+\delta}$ can also be prepared. Demazeau *et al.* (12) first mentioned the existence of $EuSrNiO_4$ ($x = 1.0$). Recently, we reported studies on the strontium-substituted samarium nickelate $Sm_{2-x}Sr_xNiO_{4+\delta}$ (4).

This work focuses on studies of the preparation of $Eu_{2-x}Sr_xNiO_{4+\delta}$ ($0.5 \le x \le 1.2$), of the refinement of their crystal structure by Rietveld analysis, and of the measurement of their infrared spectra and reducibility. The effects of Sr substitution on the structural parameters are also discussed.

[1]To whom correspondence should be addressed.

EXPERIMENTAL

A. Preparation of $Eu_{2-x}Sr_xNiO_{4+\delta}$

$Eu_{2-x}Sr_xNiO_{4+\delta}$ ($x = 0.3$, 0.5, 0.6, 0.7, 0.8, 0.9, 1.0, 1.1, 1.2, 1.5, and 1.7) samples were prepared by a citric acid complex decomposition method (13). Briefly, an aqueous solution of mixed metal nitrates with an equivalent amount of citric acid was evaporated at 332–352 K to obtain a gel. The precursors were then decomposed at 920 K for 4 h, followed by grinding, pelletizing, and calcining in air at 1533 K for 10 h.

B. Composition Determination

The metal ion composition was determined by inductively coupled plasma spectrometry (ICP) (USA Leeman, Plasma Spec I).

C. Crystal Structure Characterization

XRD data for Rietveld refinement were collected on a Rigaku D/max-3B powder diffractometer with Bragg–Brentano geometry using graphite-monochromated Cu$K\alpha$ radiation (40 kV, 30 mA) and a scintillation detector. The intensity data were collected at 298 K over a 2θ range from 10 to 130° with a step interval of 0.02° and a counting time of 8 s per step. The *d*-spacings were corrected for systematic errors by calibration with standard silicon powder ($a = 5.4309$ Å). The Rietveld refinement was performed using the program WYRLET (M. Schneider, a modified version of the program by Wiles and Young, 1981) (14). Space groups *Fmmm* and *I4/mmm* with the structural parameters of a K_2NiF_4 type compound were used as starting models. Peaks were modeled using the pseudo-Voigt profile function

0022-4596/98 $25.00

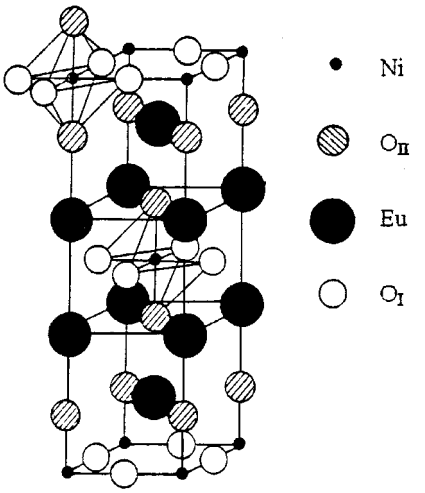

FIG. 1. K_2NiF_4 type structure of A_2BO_4.

in which a peak asymmetry parameter was included for peaks up to $2\theta = 50°$. The background parameters were modeled using a refinable fourth-order polynomial. The occupation number of atoms for all sites was fixed and was not refined.

D. Determination of Ni^{3+} Content

The percentage Ni^{3+} content, relative to the total nickel in the samples, was determined iodometrically (6, 15). Briefly, about 150 mg of an accurately weighed sample was added to a three-necked spherical flask kept under a N_2 flow and containing 30 cm^3 of 0.5 mol dm^{-3} HCl and 600 mg of KI (both in excess), and the flask was kept in the dark until the solid was completely dissolved. The solution was then quickly titrated with 0.01 mol dm^{-3} $Na_2S_2O_3$. From the values of the mean oxidation number, the percentage of Ni^{3+} in the sample was readily calculated and values are given in Table 6.

E. IR Measurement

The IR spectra were taken on a Perkin-Elmer 683 spectrophotometer. Samples were produced in the form of KBr pellets.

F. Temperature-Programmed Reduction (TPR)

Samples of $Eu_{2-x}Sr_xNiO_{4+\delta}$ (about 5 mg) were placed in a quartz reactor which was connected to a conventional TPR apparatus (15). The reduction gas employed was 10% (v/v) hydrogen in nitrogen (flow rate, 20 ml min^{-1}). During the TPR performance, the reactor was heated from room temperature to 1173 K at 20 ml min^{-1}.

RESULTS AND DISCUSSION

A. Compositions and Phases of $Eu_{2-x}Sr_xNiO_{4+\delta}$

Table 1 lists the compositions of metal ions in the samples as measured by ICP. It can be seen that the results do not deviate significantly from the starting compositions. Table 2 lists the phase characterization results of $Eu_{2-x}Sr_xNiO_{4+\delta}$ obtained from XRD. Single-phase K_2NiF_4 type compounds were obtained within the Sr^{2+} substitution range $x = 0.5$–1.2. Because of the limitation of the tolerance factor ($t = r_A/r_B$), K_2NiF_4 type structure compounds can only be produced for those with t values within the range 1.7–2.4. According to the values of the tolerance factor based on Shannon's ionic radii (17) as listed in Table 3, neodymium is the smallest rare earth metal which can form a K_2NiF_4 type lanthanide nickelate, Nd_2NiO_4. Since Eu is smaller than Nd, it cannot form a K_2NiF_4 type compound. Demazeau's work (12), our previous work (4), and this work, however, show that it is possible for Eu^{3+} to form K_2NiF_4 type compounds $Eu_{2-x}Sr_xNiO_{4+\delta}$ by partial substitution of alkaline earth metals (A) with larger radii ion such as Sr^{2+} to increase r_A or by oxidizing B ions to a higher oxidation state to decrease r_B. For $x < 0.5$, Sr^{2+} substitution is not sufficient to incorporate all Eu^{3+} and Ni^{2+} into the K_2NiF_4 type structure and some Eu_2O_3 and NiO remain as separate phases (Table 2). When Sr^{2+} substitution is above 1.5, single-phase samples cannot be obtained because of geometric factors and charge balance considerations. The excess of Sr and Ni remains as $SrCO_3$ and NiO, respectively.

B. Structure of $Eu_{2-x}Sr_xNiO_{4+\delta}$ ($0.5 \leq x \leq 1.2$)

The powder X-ray diffraction patterns of the samples can be indexed based on orthorhombic symmetry with space group *Fmmm* ($x = 0.5$–0.6) and tetragonal symmetry with space group *I4/mmm* ($x = 0.7$–1.2). The agreement between the observed and calculated powder X-ray diffraction profiles of sample $x = 0.6$ in the final refinement is shown in Fig. 2.

TABLE 1
Weight Percentage of Eu, Sr, and Ni Ions and Compositions in $Eu_{2-x}Sr_xNiO_{4+\delta}$ Determined by ICP[a]

x	Eu	Sr	Ni
0.5	57.95 (57.79)	11.18 (11.11)	14.82 (14.88)
0.6	54.96 (54.83)	13.59 (13.55)	15.20 (15.13)
0.8	48.36 (48.61)	18.88 (18.68)	15.69 (15.68)
1.0	41.98 (41.95)	24.53 (24.19)	16.26 (16.20)
1.2	34.79 (34.79)	30.07 (30.09)	16.84 (16.80)

[a]Data in parentheses are calculated values.

TABLE 2
Crystallographic Characterization of $Eu_{2-x}Sr_xNiO_{4+\delta}$

x	Phase composition	a (Å)	b (Å)	c (Å)	Space group
0.3	Eu_2O_3, NiO, $Eu_{2-x}Sr_xNiO_{4+\delta}$ ($0.3 \le x \le 0.5$)				
0.5	$Eu_{1.5}Sr_{0.5}NiO_{4+\delta}$	5.2980(1)	5.3658(1)	12.2743(2)	*Fmmm*
0.6	$Eu_{1.4}Sr_{0.6}NiO_{4+\delta}$	5.3073(1)	5.3340(1)	12.2864(2)	*Fmmm*
0.7	$Eu_{1.3}Sr_{0.7}NiO_{4+\delta}$	3.7611(1)		12.2825(1)	*I*4/*mmm*
0.8	$Eu_{1.2}Sr_{0.8}NiO_{4+\delta}$	3.7698(1)		12.2398(2)	*I*4/*mmm*
0.9	$Eu_{1.1}Sr_{0.9}NiO_{4+\delta}$	3.7715(1)		12.2265(2)	*I*4/*mmm*
1.0	$Eu_{1.0}Sr_{1.0}NiO_{4+\delta}$	3.7796(1)		12.1986(1)	*I*4/*mmm*
1.2	$Eu_{0.8}Sr_{1.2}NiO_{4+\delta}$	3.7859(1)		12.1814(1)	*I*4/*mmm*
1.5	$Eu_{2-x}Sr_xNiO_{4+\delta}$ ($1.2 < x < 1.5$), $SrCO_3$				
1.7	$Eu_{2-x}Sr_xNiO_{4+\delta}$ ($1.2 < x < 1.7$), $SrCO_3$, NiO				

The lattice parameters a, b, and c obtained are listed in Table 2. With increasing x, c reached a maximum at around $x = 0.6$, which is similar to the systems $Ln_{2-x}Sr_xNiO_{4+\delta}$ (Ln = La, Nd, and Sm) (4, 10, 11, 18). As indicated in Table 2, there is a crystal system transformation at around $x = 0.6$–0.7.

Tables 4 and 5 list structure parameters and interatomic distances for the $Eu_{2-x}Sr_xNiO_{4+\delta}$. It is noted with great interest that the bond length of Ni–O_{II}($\parallel c$-axis) monotonously decreases with increasing x without exhibiting any anomaly at $x = 0.6$–0.7 as expected from the variation of the parameter c, which indicates that the Jahn–Teller distortion of the NiO_6 octahedron along the c-axis monotonously decreases with increasing x. This can also be confirmed by the bond length ratio of Ni–O_{II}($\parallel c$-axis) to NiO_I($\parallel a$-axis) as shown in Table 5.

The bond length change percentage, Δ, defined as $(d_{max} - d_{min})/d_{min}$, within the x range 0.5–1.2 was used to

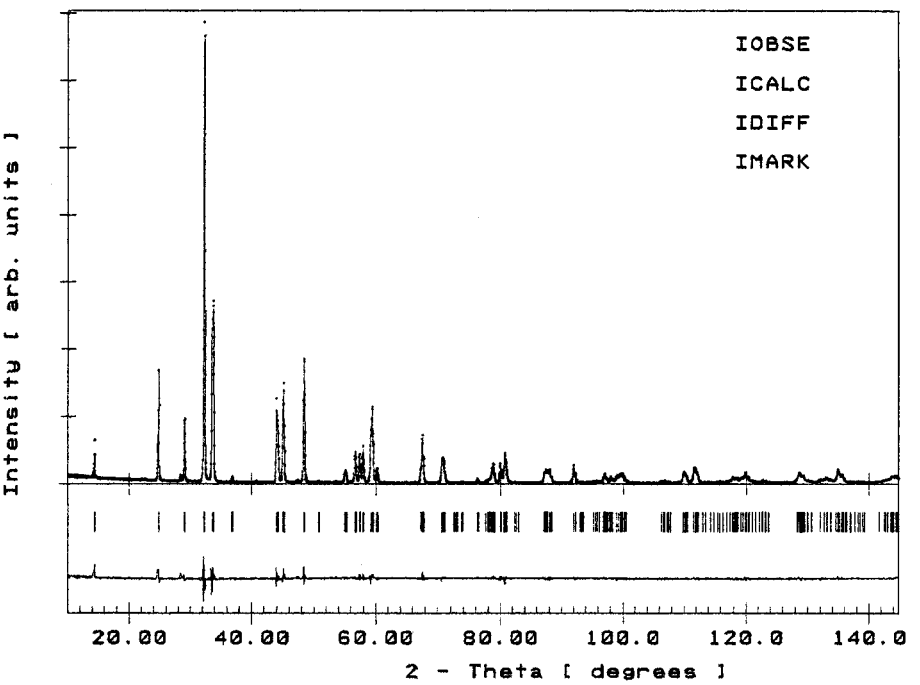

FIG. 2. Rietveld refinement patterns for $Eu_{1.4}Sr_{0.6}NiO_{4+\delta}$. The observed data are indicated by dots and the calculated data by the solid line overlaying them. The short vertical lines mark the positions of possible Bragg reflections, and the lower curve shows the difference between the observed and calculated powder diffraction patterns.

TABLE 3
Values of the Tolerance Factor ($t = r_A/r_B$) of Nd^{2+}, Eu^{3+}, and Sr^{2+} with Different Valence Values of Ni Ions Based on Shannon's Ionic Radii

	Nd^{2+}	Eu^{3+}	Sr^{2+}
Ni^{2+}	1.69	1.62	1.90
Ni^{3+} (low spin)	2.08	2.00	2.30
Ni^{3+} (high spin)	1.94	1.87	2.20

present the variation extent of interatomic distances as shown in Table 5. The data can roughly be divided into two regions. In the first region Δ values for Ni–O_I($\parallel a$-axis), Eu(Sr)–O_I, Eu(Sr)–Eu(Sr)($\parallel c$-axis), and Eu(Sr)–Ni($\parallel c$-axis) are all less than 1%, whereas in the second region Δ values for Ni–O_{II}($\parallel c$-axis) and Eu(Sr)–O_{II}($\parallel c$-axis) are around 5%, which is almost 10 times as much as those in the first region. This indicates that there is a rigid NiO_4 network parallel to the a, b plane which is affected very little by Sr substitution, whereas Sr substitution causes a drastic shift of O_{II} ions from Eu(Sr) toward Ni while the Eu(Sr)–Ni distance along the c-axis remains essentially unaltered.

TABLE 4
Positional and Thermal Parameters for $Eu_{2-x}Sr_xNiO_{4+\delta}$

			x	
Atom	Site	Parameter	0.5	0.6
Eu, Sr	8*i*	*z*	0.3603(1)	0.3603(1)
		B (Å^2)	0.56(2)	0.39(1)
Ni	4*a*	*B* (Å^2)	0.22(6)	0.16(5)
O_I	8*e*	*B* (Å^2)	1.40(20)	0.87(14)
O_{II}	8*i*	*z*	0.1746(6)	0.1721(5)
		B (Å^2)	2.50(24)	2.37(19)
Residuals (%)		R_{wp}	12.85	12.14
		R_p	8.98	8.57
		R_E	2.81	2.60
		R_I	3.60	4.05

			x				
Atom	Site		0.7	0.8	0.9	1.0	1.2
Eu, Sr	4*e*	*z*	0.3604(1)	0.3606(1)	0.3607(1)	0.3605(1)	0.3603(1)
		B (Å^2)	0.39(1)	0.40(2)	0.43(1)	0.42(2)	0.12(1)
Ni	2*a*	*B* (Å^2)	0.23(4)	0.33(6)	0.35(5)	0.32(6)	0.31(3)
O_I	4*c*	*B* (Å^2)	0.86(12)	0.62(15)	0.92(13)	1.07(6)	0.62(11)
O_{II}	4*e*	*z*	0.1712(4)	0.1676(5)	0.1675(5)	0.1660(5)	0.1651(4)
		B (Å^2)	1.56(14)	1.58(18)	1.70(16)	1.58(15)	1.24(13)
Residuals (%)		R_{wp}	10.87	13.88	11.73	14.03	11.67
		R_p	7.78	9.05	8.35	8.82	7.02
		R_E	2.37	3.17	2.71	0.72	2.76
		R_I	3.06	4.37	3.35	4.50	3.86

The shift of the O_{II} ions from Eu(Sr) toward Ni ions may arise for two reasons. On the one hand, the bond strength of M–O can be presented in terms of the sum of the M–O bond formation enthalpies $\sum(\Delta H_{M-O})$ in the solids (19). Table 6 lists calculated results. It can be seen that $\sum(\Delta H_{A-O})$ decreases with increasing x, which indicates that the acidity of the A ions decreases and the strength of the A–O covalent bond reduces as Sr is substituted. On the other hand, after partial substitution of Eu^{3+} by Sr^{2+}, some Ni^{2+} ions are oxidized to Ni^{3+} to meet charge balance considerations. The acidity of the B ion then increases, and its covalent bond to oxygen becomes stronger. It is the combination of these effects that causes O_{II} to shift from Eu(Sr) toward Ni ions.

The concept of bond valence has recently found wide applicability in solid-state chemistry. The main advantage of the approach is that, to a generally excellent approximation, the bond length is a unique function of bond valence. The most commonly adopted empirical expression has been proposed for valence calculations as $V_i = \sum_j v_{ij} = \sum_j \exp[(R_{ij} - d_{ij})/b]$ (20), for which V_i is the valence of atom i, v_{ij} is the valence of a bond between two atoms i and j, R_{ij} is the bond-valence parameter, d_{ij} is the bond length of Ni–O_I or Ni–O_{II}, and b is a universal constant (0.37 Å). The R parameters for Ni^{2+}–O and for low-spin Ni^{3+}–O are 1.654 and 1.68 Å, respectively. The V_i values calculated according to the content of Ni^{2+} and Ni^{3+} are listed in Table 6. Figure 3 shows that the bond valence of Ni increases with increasing x in the $Eu_{2-x}Sr_xNiO_{4+\delta}$ system. The curve bends at around $x = 0.6$–0.7, which is in agreement with the fact that there is a crystal system transformation at around $x = 0.6$.

IR spectra of $Eu_{2-x}Sr_xNiO_{4+\delta}$ are shown in Fig. 4. There are three main absorption bands at about 705, 520, and 400 cm^{-1}, which are assigned to the symmetric stretching of Eu(Sr)–O_{II}–Ni($\parallel c$-axis) and the asymmetric stretching and bending modes of the Ni–O_I linkages in the basal planes,

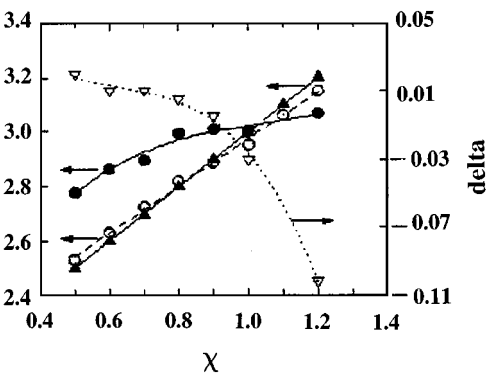

FIG. 3. Average bond valence (●), measured mean oxidation number (○), and calculated mean oxidation number (△) of Ni and δ (▽) as functions of x in $Eu_{2-x}Sr_xNiO_{4+\delta}$.

TABLE 5
Interatomic Distances of $Eu_{2-x}Sr_xNiO_{4+\delta}$

	x							
Distance (Å)	0.5	0.6	0.7	0.8	0.9	1.0	1.2	Δ%
$Ni–O_I$ ($\|a$-axis)	1.885(1)	1.881(1)	1.881(1)	1.885(1)	1.886(1)	1.890(1)	1.893(1)	0.638
$Ni–O_{II}$ ($\|c$-axis)	2.143(8)	2.115(6)	2.103(5)	2.081(6)	2.068(5)	2.045(6)	2.011(5)	6.56
$Eu–O_{II}$ ($\|c$-axis)	2.280(8)	2.312(6)	2.324(5)	2.362(6)	2.362(5)	2.373(6)	2.378(5)	4.30
$Eu–O_I$	2.548(1)	2.547(1)	2.545(1)	2.542(1)	2.541(1)	2.543(1)	2.545(1)	0.275
Eu–Eu ($\|c$-axis)	3.770(1)	3.763(1)	3.761(1)	3.770(1)	3.775(1)	3.780(1)	3.786(1)	0.665
Eu–Ni ($\|c$-axis)	3.184(1)	3.172(1)	3.164(1)	3.165(1)	3.166(1)	3.168(1)	3.172(1)	0.664
$Ni–O_{II}/Ni–O_I$	1.137	1.124	1.118	1.104	1.097	1.082	1.063	

respectively (21, 22). All the absorption bands become weaker with increasing x, which is consistent with the decrease of the Jahn–Teller distortion of the NiO_6 octahedron and the increase of symmetry of the crystal structure, as discussed earlier.

C. Valence State of Nickel in $Eu_{2-x}Sr_xNiO_{4+\delta}$

The mean oxidation number of nickel in the samples is shown as a function of Sr content in Fig. 3. The Ni^{3+} content, oxygen nonstoichiometry (δ) calculated from the mean oxidation number of nickel and occupancy (equal to unity), and the formula of $Eu_{2-x}Sr_xNiO_{4+\delta}$ are listed in Table 6. It can be seen that the valence state of nickel in the samples does not deviate much from theoretical data. Therefore, the valence state of B ions in A_2BO_4 compounds can be easily controlled by substitution of A ions by A'. In this study, the mean oxidation number of nickel can even be above 3 (3.06 and 3.16 for $x = 1.1$ and $x = 1.2$, respectively). These properties should be important in catalysis studies.

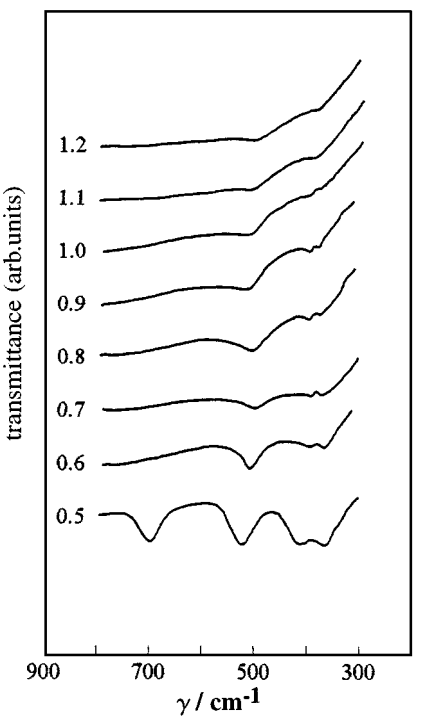

FIG. 4. Infrared absorption spectra of $Eu_{2-x}Sr_xNiO_{4+\delta}$ ($x = 0.5$–1.2).

D. Reducibility of $Eu_{2-x}Sr_xNiO_{4+\delta}$

TPR profiles of $Eu_{2-x}Sr_xNiO_{4+\delta}$ are shown in Fig. 5. There are two reduction peaks in the TPR profile for each sample. After the lower temperature reduction, the K_2NiF_4 structure still remains stable although some Ni ions are reduced. The higher temperature reduction peak leads to the total reduction of Ni ions in the sample and the K_2NiF_4 structure is destroyed (23). The reducibility of the sample is probably determined by the stability of the NiO_6 octahedron in the system. Table 7 lists the reduction peak temperatures (T_{max}), the hydrogen uptakes, and the reduction percentage of the two peaks. The reduction percentage of

TABLE 6
Average Bond Valence of Ni, Content of Ni^{3+}, δ, and Sum of the M–O Bond Formation Enthalpies [$\sum(\Delta H_{M-O})$] in $Eu_{2-x}Sr_xNiO_{4+\delta}$

x	Average bond valence of Ni	Content of Ni^{3+} (%)[a]	δ	$\sum(\Delta H_{A-O})$ (kJ mol^{-1})	$\sum(\Delta H_{Ni-O})$ (kJ mol^{-1})
0.5	2.78	53	0.02	466.6	68.3
0.6	2.87	63	0.01	451.7	70.3
0.7	2.90	72.5	0.01	440.9	72.3
0.8	3.00	82	0.005	427.4	74.3
0.9	3.01	89	− 0.005	416.4	75.7
1.0	3.01	95	− 0.03	403	77.0
1.2	3.07	100	− 0.102	380.4	78.0

[a] The contents of Ni^{3+} and oxygen were calculated from the mean oxidation number of the Ni ion as measured by iodometry.

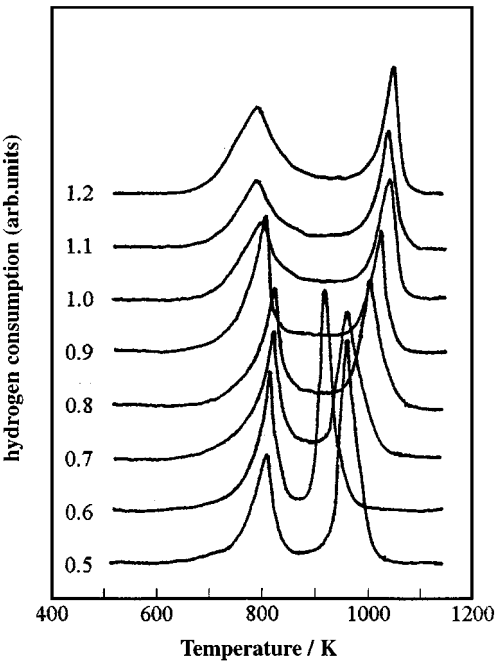

FIG. 5. TPR profiles of $Eu_{2-x}Sr_xNiO_{4+\delta}$ ($x = 0.5$–1.2).

the peaks is not consistent with the relative amounts of Ni^{2+} and Ni^{3+} in the system, which implies that they do not relate to the reduction of the different valence of Ni ions but rather relate to the reduction of oxygen with different binding energies on different sites. $T_{\max,l}$ does not vary much for the whole x range. This might relate to the constant M–O bond length. For $T_{\max,h}$, it first decreases in the range $0.5 \leq x \leq 0.6$ and then increases in the range $0.6 \leq x \leq 1.2$, which is opposite to the cell parameter c. This means that the structure stability of $Eu_{2-x}Sr_xNiO_{4+\delta}$ is related to the distance between the layers of perovskite and rock salt.

CONCLUSION

K_2NiF_4 type europium nickelate can be prepared by partial substitution of Sr^{2+} for Eu^{3+} to increase the radius of A ions and decrease the radius of B ions by oxidizing the B ions into a higher valence state. The Sr^{2+} substitution causes a drastic shift of O_{II} ions along the c-axis from Eu(Sr) toward Ni while scarcely affecting the NiO_4 in the basal plane and the Eu(Sr)–Ni distance along the c-axis. The Jahn–Teller distortion of the NiO_6 octahedron decreases with increasing x without any minimum from $x = 0.5$ to $x = 1.2$. The variation of the higher peak temperature on the TPR profiles with x is opposite to the variation of the cell parameters c, which indicates that the structural stability of $Eu_{2-x}Sr_xNiO_{4+\delta}$ is related to the distance between the layers of perovskite and rock salt.

TABLE 7
TPR Measurements on $Eu_{2-x}Sr_xNiO_{4+\delta}$

x	$T_{\max,l}$ (K)	V_l (m mol g^{-1})	Reduction (%)	$T_{\max,h}$ (K)	V_h (m mol g^{-1})	Reduction (%)
0.5	818	1.51	39.0	988	2.31	61.0
0.6	828	1.48	41.3	943	2.11	58.7
0.7	828	2.10	49.7	973	2.13	50.3
0.8	828	1.88	48.4	1023	2.00	51.6
0.9	808	1.71	48.4	1038	1.83	51.6
1.0	808	2.32	48.4	1063	2.47	51.6
1.1	798	2.58	50.9	1058	2.48	49.1
1.2	798	2.81	55.3	1068	2.27	44.7

ACKNOWLEDGMENTS

The authors acknowledge the financial support of the Natural Science Foundation of Zhejiang Province, China. They also thank Mei Minghua for experimental help.

REFERENCES

1. P. Ganguly and C. N. R. Rao, *Mater. Res. Bull.* **8,** 405 (1973).
2. B. W. Arbuckle, K. V. Ramanujachary, Z. Zhang, and M. Greenblatt, *J. Solid State Chem.* **88,** 278 (1990).
3. B. W. Arbuckle, K. V. Ramanujachary, A. M. Buckley, and M. Greenblatt, *J. Solid State Chem.* **97,** 274 (1992).
4. H. Lou, Y. Ge, P. Chen, F. Ma, and G. Lü, *J. Mater. Chem.* **7,** 2097 (1997).
5. M. Sayer and P. Odier, *J. Solid State Chem.* **67,** 26 (1987).
6. C. N. R. Rao, P. Ganguly, K. K. Singh, and R. A. Mohan Ram, *J. Solid State Chem.* **72,** 14 (1988).
7. A. K. Ladavos and P. Pomonis, *J. Chem. Soc., Faraday Trans.* **87,** 3291 (1991).
8. T. Nitadori, M. Muramatsu, and M. Misono, *Bull. Chem. Soc. Jpn.* **61,** 3831 (1988).
9. D. Ganguli, *J. Solid State Chem.* **30,** 353 (1979).
10. Y. Takeda, R. Kanno, M. Sakano, O. Yamamoto, M. Takano, Y. Banndo, H. Akinaga, K. Takita, and J. B. Goodenough, *Mater. Res. Bull.* **25,** 293 (1990).
11. Y. Takeda, M. Nishijima, N. Imanishi, R. Kanno, O. Yamamoto, and M. Takano, *J. Solid State Chem.* **96,** 72 (1992).
12. G. Demazeau, M. Pouchard, and P. Hagenmuller, *J. Solid State Chem.* **18,** 159 (1976).
13. M. S. G. Baythoun and F. R. Sale, *J. Mater. Sci.* **17,** 2757 (1982).
14. A. Sakthivel and R. A. Young, "User's Guide to Programs DBWS-9006," 1981.
15. B. E. Gushee, L. Katz, and R. Ward, *J. Am. Chem. Soc.* **79,** 5061 (1957).
16. A. Jones and B. D. McNicol, *in* "Temperature-Programmed Reduction for Solid Materials Characterization," p. 105. Marcel/Dekker. New York, 1986.
17. R. D. Shannon, *Acta Crystallogr., Sect. A* **32,** 751 (1976).
18. H. Zheng, S. Du, G. Lu, H. Lou, and F. Ma, *Acta Chim. Sin.* **51,** 373 (1993).
19. A. K. Ladavos and P. J. Pomonis, *Appl. Catal. B* **1,** 101 (1992).
20. N. E. Brese and M. O'Keeffe, *Acta Crystallogr., Sect. B* **47,** 192 (1991).
21. K. K. Singh, P. Ganguly, and J. B. Goodenough, *J. Solid State Chem.* **52,** 254 (1984).
22. Y. Wu, Z. Yu, and S. Liu, *J. Solid State Chem.* **112,** 157 (1994).
23. H. Lou, F. Ma, and Y. Chen, *React. Kinet. Catal. Lett.* **42,** 151 (1990).